HHS Public Access

Author manuscript

Biomaterials. Author manuscript; available in PMC 2020 February 01.

Published in final edited form as:

Biomaterials. 2019 February ; 192: 560–568. doi:10.1016/j.biomaterials.2018.10.040.

Microfluidic-enabled bottom-up hydrogels from annealable naturally-derived protein microbeads

Amir Sheikhi[1,2,3], **Joseph de Rutte**[1], **Reihaneh Haghniaz**[1,2,3], **Outman Akouissi**[1,2,3], **Alireza Sohrabi**[1], **Dino Di Carlo**[1,3,4,*], and **Ali Khademhosseini**[1,2,3,4,5,6,7,8,*]

[1]Department of Bioengineering, University of California - Los Angeles, 410 Westwood Plaza, Los Angeles, CA 90095, USA

[2]Center for Minimally Invasive Therapeutics (C-MIT), University of California - Los Angeles, 570 Westwood Plaza, Los Angeles, CA 90095, USA

[3]California NanoSystems Institute (CNSI), University of California - Los Angeles, 570 Westwood Plaza, Los Angeles, CA 90095, USA

[4]Jonsson Comprehensive Cancer Centre, University of California - Los Angeles, 10833 Le Conte Ave, Los Angeles, CA 90024, USA

[5]Department of Radiological Sciences, David Geffen School of Medicine, University of California - Los Angeles, 10833 Le Conte Ave, Los Angeles, CA 90095, USA

[6]Department of Chemical and Biomolecular Engineering, University of California - Los Angeles, 5531 Boelter Hall, Los Angeles, CA 90095, USA

[7]Department of Bioindustrial Technologies, College of Animal Bioscience and Technology, Konkuk University, Seoul, 143-701, Republic of Korea

[8]Center of Nanotechnology, Department of physics, King Abdulaziz University, Jeddah, 21569, Saudi Arabia

Abstract

Naturally-derived proteins, such as collagen, elastin, fibroin, and gelatin (denatured collagen) hold a remarkable promise for tissue engineering and regenerative medicine. Gelatin methacryloyl (GelMA), synthesized from the methacryloyl modification of gelatin, mimicking the structure of extracellular matrix, has widely been used as a universal multi-responsive scaffold for a broad spectrum of applications, spanning from cell therapy to bioprinting and organoid development. Despite the widespread applications of GelMA, coupled stiffness and porosity has inhibited its applications in 3D cellular engineering wherein a stiff scaffold with large pores is demanded (e.g.,

*Corresponding authors: Dino Di Carlo (dicarlo@g.ucla.edu), Ali Khademhosseini (khademh@ucla.edu).

Conflicts of interest

There are no conflicts of interest to declare.

Data availability

The raw/processed data required to reproduce these findings are available upon request.

at concentrations >10 wt%). Taking advantage of the orthogonal thermo-chemical responsivity of GelMA, we have developed microfluidic-assisted annealable GelMA beads, that are first stabilized by temperature-mediated physical crosslinking, flowed to form a scaffold structure, and then chemically annealed using light to fabricate novel bead-based 3D GelMA scaffolds with high mechanical resilience. We show how beaded GelMA (B-GelMA) provides a self-standing microporous environment with an orthogonal void fraction and stiffness, promoting cell adhesion, proliferation, and rapid 3D seeding at a high polymer concentration (~20 wt%) that would otherwise be impossible for bulk GelMA. B-GelMA, decorated with methacryloyl and arginylglycylaspartic acid (RGD) peptide motifs, does not require additional functionalization for annealing and cell adhesion, providing a versatile biorthogonal platform with orthogonal stiffness and porosity for a myriad of biomedical applications. This technology provides a universal method to convert polymeric materials with orthogonal physico-chemical responsivity to modular platforms, opening a new horizon for converting bulk hydrogels to beaded hydrogels (B-hydrogels) with decoupled porosity and stiffness.

Graphical Abstract

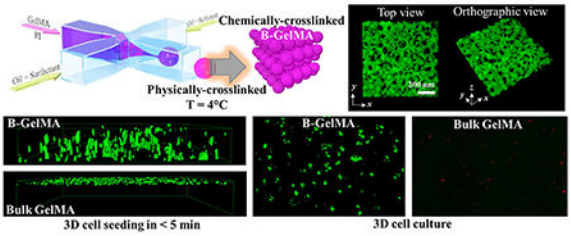

Keywords

Gelatin methacryloyl (GelMA); modular hydrogels; microporous scaffolds; microbeads; 3D cell seeding; particle gels

Introduction

Hydrogels, hydrophilic polymer networks that may absorb water up to several orders of magnitude higher than their dry mass, have secured a promising role in developing cell microenvironments for tissue engineering [1–8]. Common strategies to build hydrogel scaffolds for biomedical applications encompass chemical crosslinking and physical bonding [9,10], enabling permanent and/or reversible network formation for controlled delivery of target cells and cargos [11–17]. In the past few decades, significant effort has been devoted to design, synthesize, and engineer hydrogels at the micro- and nanoscale to impart unique properties, such as surface patterns, injectability, and stimuli-responsiveness [18–22]. These properties are typically applied to “bulk” hydrogels, wherein one or several types of building blocks (e.g., polymer chains and/or nanoparticles) interact throughout the whole network, leaving no connected voids or other openings among the constituents at the microscale.

To obtain a micron-sized characteristic mesh size ξ, the storage modulus of the hydrogel $G' \sim k_B T/\xi^3$ is in the order of mPa, an implausibly low modulus, in which random micron-sized pores would also be randomly arranged without interconnectivity. Here, k_B is the Boltzmann constant ($\sim 1.38\times10^{-23}$ m^2 kg s^{-2} K^{-1}), and T denotes temperature [23]. On the other hand, stiff hydrogels, often demanded in a variety of tissue engineering applications, including bone and muscle tissue engineering, may not provide a favorable microenvironment for cells, due to the small mesh size, impaired nutrient and oxygen permeation, and the stress exerted to the encapsulated cells during the polymer network formation.

Lack of pore interconnectivity in “bulk” hydrogels, inhibiting effective cell elongation, migration, and polarization has stimulated an immense interest towards developing microporous scaffolds based on small-scale gel building blocks, such as microspheres. To address some of the challenges associated with bulk hydrogels, droplet microfluidic-assisted small-scale gel particle fabrication has emerged for biomedical applications [24]. Recently, microporous annealed particle (MAP) gels have emerged through a two-step chemical reaction cascade, involving (i) the chemical crosslinking of individual micron-sized beads made up of synthetic materials followed by (ii) the chemical annealing of beads into a larger interconnected scaffold. Multi-armed poly(ethylene) glycol-vinyl sulfone microbeads, decorated with arginylglycylaspartic acid (RGD) cell adhesive peptide motifs and tissue adhesive peptides have been crosslinked through the Michael-type addition with cysteine-terminated matrix metalloprotease (MMP)-sensitive peptide sequences [25]. The individually crosslinked beads were annealed via the covalent bonding between the K (Ac-FKGGERCG-NH_2) and Q (Ac-NQEQVSPLGGERCG-NH_2) peptides obtained by activated Factor XIII (FXIIIa).

Hyaluronic acid (HA) has also been used as a platform for producing bead-based hydrogels. Acrylamide-modified HA has been doped with SH-containing pendent peptides, namely Q and K peptides, which was mixed with dithiol matrix metalloproteinase (MMP)-sensitive linker peptide (Ac-GCRDGPQGIWGQDRCG-NH_2), annealed using FXIIIa and thrombin, star PEG-N-acryloxysuccinimid (NHS), or white light-activated Eosin Y [26]. The chemical annealing methods required up to 90 min to complete, while the light-mediated strategy took place in ~ 1 min. Host-guest interactions among the beads have been adapted to reduce chemical complexity and impart reversibility to the bead-bead binding, allowing for a shear-thinning behavior. Photoinitiated thiol-ene reaction of norbornene-modified HA with a di-thiol crosslinker (dithiotritiol, DTT) yielded individually-crosslinked beads, which where reversibly annealed using adamantane-cyclodextrin guest-host binding [27]. This technology, however, demands the off-chip UV light curing of individual (non-annealed) beads, which may introduce additional complexity to controlling the shape, stiffness, and homogeneity of the beads. Crosslinking beads in the oil phase is highly prone to oxygen quenching as a result of a sharp oxygen gradient within the beads [28], which may result in heterogenous stiffness.

Here, we introduce a facile, universal strategy to convert thermo-sensitive materials with crosslinkable moieties into bead-based scaffolds. As an important model biomaterial, we have selected a naturally-derived protein, gelatin (denatured collagen), which has a broad range of biomedical applications for tissue engineering and regeneration [29–33], benefitting

from built-in RGD peptides, tissue adhesiveness, and thermo-sensitivity. Gelatin, modified with methacrylic anhydride (MA), known as GelMA has been widely used as a photocrosslinkable biomaterial to mimic the extracellular matrix (ECM), owing to its inherited properties from collagen, ECM's most abundant structural protein. Unique properties of GelMA, including cell and tissue binding cues, biocompatibility, bioactivity, tunable stiffness and biodegradation, cost effectiveness, and facile synthesis have been explored in a broad spectrum of applications, from tissue engineering to wound healing, cargo delivery, soft lithography and microfabrication [34–37].

We show that GelMA, a photocrosslinkable, thermo-responsive protein derivative, may be produced in the form of microbeads using a flow focusing microfluidic device and be readily purified from the oil/surfactant coating in a cold aqueous environment without any chemical reaction, in contrast to all of the existing [25–27] annealable beaded platforms, which make use of chemical crosslinking before the purification. The photochemically-active, physically-crosslinked beads are then crosslinked and annealed to each other through UV light exposure in the aqueous phase, yielding a beaded GelMA (B-GelMA) scaffold with interconnected pores. We shed light on the key advantages of the B-GelMA platform over conventional (bulk) GelMA by investigating their mechanical, rheological, and biological characteristics. B-GelMA, providing orthogonal void fraction and stiffness provides a novel platform for 3D cellular engineering, e.g., fibroblasts and endothelial cells, using stiff matrices (e.g., GelMA ~ 20 %w/v) without compromising cell viability, which may otherwise be impossible. Promising cell viability, adhesion, proliferation, elongation, and seeding inside stiff B-GelMA may set the stage for the next generation of ECM-mimicking microporous cell scaffolds for accelerated healing and regeneration.

Materials and methods

Materials and methods are detailed in a parallel publication [38]. Briefly, a flow focusing device was fabricated from polydimethylsiloxane (PDMS) using soft lithography to produce a water-in-oil emulsion containing GelMA with a high degree of methacryloyl substitution and a photoinitiator (PI, Irgacure 2959, 0.5% w/v) in the aqueous phase and Novec 7500 oil-surfactant (0.5 wt% PicoSurf) mixture in the oil phase. Surfactant-stabilized micron-sized GelMA beads in the oil were produced and physically-crosslinked by decreasing temperature to 4°C, followed by breaking the emulsion using a 20% perfluorooctanol solution in Novec 7500 oil and removing the oil through pulse centrifugation, the decantation of supernatant, and the addition of cold (4°C) DPBS. The physically-stabilized microbeads were resuspended in cold DPBS including PI, readily injected using a positive displacement pipette, crosslinked and annealed to neighboring microbeads via UV light exposure.

Results and discussion

The flow focusing microfluidic device is able to effectively produce uniform-sized GelMA microbeads, through pinching the aqueous phase with oil/surfactant flows, as presented schematically in Figure 1a. The microbeads are then collected as a disperse phase in a continuous oil phase, which may be readily purified by a secondary surfactant after

physically crosslinking the beads at 4 °C. This initial physical crosslinking step is essential to prevent the dissolution of beads once they are transferred into an aqueous medium, allowing for the elimination of any chemical/light treatment, which have frequently been required in other beaded systems, such as HA [26,27] and poly(ethylene) glycol-vinyl sulfone [25]. The purified beads may undergo subsequent chemical crosslinking using various mechanisms, such as UV-light mediated radical polymerization, forming an annealed 3D scaffold with permanent microporosity. The microfluidic setup, comprising flow focusing device to generate the GelMA beads and a reservoir for bead collection is shown in Figure 1b.

The capability of the microfluidic flow focusing device to generate GelMA beads with various sizes was explored by changing the GelMA solution (aqueous phase) concentration and the ratio of oil to aqueous flow rates. Figure 1c presents the size of oil/surfactant-stabilized beads versus the ratio of oil to aqueous flow rates. The beads with 7% (w/v) GelMA content were produced in the range of ~ 70 – 120 μm. Smaller beads are generated at higher oil-to-water flow ratios, as a result of increased pinching of the aqueous phase by the oil flow. A flow focusing device allows for a wide range of bead size production with a simple microfluidic device, only by tuning the flow. Increasing the polymer concentration to 10% and 20% (w/v) slightly decreases the maximum bead size to ~ 112 and 105 μm, respectively.

The stability of the physically-crosslinked beads is a critical factor in designing advanced structures, because it regulates the “allowed” processing time, defined as the maximum time that beads may hold their shape and integrity in an aqueous medium. Figure 2a presents the time-evolution of physically-crosslinked GelMA microbead sizes (diameter) at various temperatures. At 4 °C, the beads hold their shape for up to at least 6 h, showing no significant change in their diameter. After 12 h, the bead diameter increases by ~ 15%, which may be because of the partial swelling. At room temperature (25°C), the beads are more susceptible to temperature and can maintain their size only for about 3 min. After 10 min, 30 min, and 1 h, the size increases by ~ 7%, 20%, and 45% respectively. After 1 h, the beads are highly swollen and ready for dissolution in the medium, which makes them hardly observable. The sensitivity to temperature is more severe at physiological temperature, resulting in a complete dissolution of beads in less than 7 min at 37°C. The results may be explained by the sol-gel transition temperature of GelMA, originated from the temperature-dependent triple helix formation [39] of denatured collagen fibers at 31-32°C [40]. This behavior is of utmost importance in designing structured scaffolds from the microbead building blocks.

To investigate the stability of chemically-crosslinked microbeads at physiological conditions, a diluted monolayer of beads, containing the PI was exposed to UV light for 2 min in a cold DPBS-PI solution. The crosslinked beads were then incubated at 37°C for an extended time. The results, presented in Figure 2a, attest to the excellent stability of the chemically-crosslinked beads at the high temperature. The swelling and shrinkage of the crosslinked beads may be engineered through altering the osmolarity gradient between the beads and media. When the physically-crosslinked beads are loaded with 1× DPBS and placed in a 5× DPBS solution, the osmotic pressure results in the flux of water out of the

beads, shrinking the beads (Figure 2b). Oppositely, when the ionic strength inside the beads is higher than the medium, osmotic flow of water swells the beads. Ion-regulated swelling of GelMA microbeads may be exploited for designing stimuli-responsive carriers. Notably, the chemically-crosslinked beads did not undergo significant swelling or shrinking (Figure 2b).

The physically-crosslinked beads may be then assembled into a structurally sound multi-layer scaffold through packing and UV-light mediated chemical crosslinking and annealing. Figure 3a demonstrates how physically-stabilized packed microbeads in an aqueous solution undergo chemical annealing, forming a densely-packed self-standing microporous scaffold (B-GelMA). The mechanical properties of the scaffolds, play an important role in their biomedical applications. For example, injectable scaffolds for cardiac and abdominal tissue engineering must mimic the native tissues and withstand large strains and stresses of the heartbeat and other activities, such as coughing. The stiffness of left ventricle during diastole is ~10-20 kPa and it increases to 200-500 kPa when diastole finishes [41]. Importantly, the pressure in the heart may reach ~ 19 kPa in a healthy adult [42], and intra-abdominal pressure may be elevated to ~ 34 kPa [43].

The mechanical properties of B-GelMA fabricated from a 20% w/v GelMA solution in DPBS are characterized in terms of tensile and compression moduli (Figure 3b). The high mechanical resilience of B-GelMA scaffolds enables handling them for measuring tensile strength. The tensile stress versus strain for B-GelMA and GelMA scaffolds are presented in Figure 3c. When prepared similarly, e.g., 2 min of UV light-mediated crosslinking, at a certain strain, the tensile stress of B-GelMA is lower than the bulk material, possibly as a result of high microporosity and lower contact area among beads. Figure 3d presents the tensile modulus of B-GelMA and bulk scaffolds. B-GelMA attains a tensile modulus in the range of 10-30 kPa, whereas, for the bulk GelMA, the tensile modulus spans ~ 100-200 kPa, for a crosslinking time ~ 1-3 min.

The compression moduli of the scaffolds, measured from the linear fits to the stress-strain curves at strain < 10% (Figure 3e), are summarized in Figure 3f. When GelMA is not chemically crosslinked, at room temperature, it forms a physical gel with a compression modulus ~ 3 and 6 kPa for B-GelMA and bulk scaffolds, respectively. Chemical crosslinking for 60, 120, and 180 s results in the formation of mechanically resilient B-GelMA scaffolds with compression moduli ~ 25, 46, and 107 kPa, respectively. To the best of our knowledge, such a mechanical stiffness is remarkably higher than any other beaded platforms. For example, a maximum compression modulus of ~ 1 kPa is reported for acrylamide-modified HA doped with SH-containing peptides [26]. In comparison to the bulk GelMA, the compression moduli of B-GelMA scaffolds are lower by 2-5 folds.

Despite the lower compression modulus of B-GelMA scaffolds than GelMA, we investigated the local stiffness of the single beads in the annealed scaffold using AFM-assisted nanoindentation to identify the stiffness at the microscale relevant to an adhered cell. The compression modulus of the beads was measured at an indentation depth ~ 100 nm to understand the local stiffness of the scaffolds that cells may experience. Figure 3g presents the stress-strain curves of B-GelMA and GelMA, obtained through the indentation of the beads and bulk gel. As can be seen in this figure, at a certain strain, the compression

stress of beads is close to the bulk hydrogels. The compression moduli of the beads, calculated from a linear fit to the stress-strain curves are very close to the bulk gel (Figure 3h), attesting to the identical GelMA crosslinking in both types of gels.

To conduct further structural characterization, the storage G' and loss moduli G'' of B-GelMA scaffolds were measured at varying angular frequencies using a standard oscillatory rheology technique. G' and G'' versus angular frequency at an oscillatory shear strain ~ 0.1% are presented in Figures 3i and 3j, respectively. At angular frequencies below ~ 10 rad s^{-1}, the storage moduli of the scaffolds are almost independent of the frequency, showing a typical solid-like behavior. Increasing the frequency increases the storage moduli, showing a shift towards a glassy behavior [44]. Accordingly, the B-GelMA scaffolds behave like the bulk GelMA. Increasing the crosslinking time increases the viscoelastic moduli, as observed in the compression and tensile moduli. For example, at an angular frequency ~ 1 rad s^{-1}, the storage moduli ~ order of 100 and ~ 1000 Pa and loss moduli ~ order of 10 and 100 Pa were obtained for B-GelMA with a crosslinking time ~ 60 and 180 s, respectively. The bulk scaffolds attain higher viscoelastic moduli, e.g., at 180 s crosslinking time, G' ~ order of 5000 Pa and G'' ~ order of 200 Pa, respectively (Figures 3k and 3l).

The void fraction of B-GelMA with varying stiffness was measured through the 3D reconstruction of *z*-stacks, obtained from confocal microscopy of fluorescent-labelled scaffolds. A large molecular weight fluorescent dextran was incubated with the annealed B-GelMA scaffolds, diffusing into the interconnected void spaces without penetrating the beads. Figure 4a shows the 3D projection of B-GelMA scaffolds from the top and orthographic views, showing the void space, labeled in green. The *z*-stacks were individually analyzed to measure the diameter distribution of equivalent circles filling the void space (Figure 4b). The void fraction versus the crosslinking time is presented in Figure 4c. While increasing the crosslinking time increases the scaffold stiffness (Figure 3), it does not have any significant effect on the void fraction, which is ~ 15% for all scaffolds. The median pore diameter, presented in Figure 4d, has a similar trend to void fraction. Increasing the B-GelMA scaffold stiffness does not affect the pore size, and all the scaffolds attain a median pore diameter ~ 20 μm. Accordingly, B-GelMA generates a protein-based bottom-up hydrogel scaffold with orthogonal porosity and stiffness.

The biological activity of B-GelMA in hosting cells was investigated by mixing NIH/3T3 fibroblasts with physically-crosslinked GelMA beads, followed by UV light exposure for 120 s to form cell-laden B-GelMA scaffolds. A high concentration of GelMA (20% w/v) was selected to elucidate the fundamental differences between the bead-based and the bulk scaffolds. The fibroblasts were cultured for 14 days in the B-GelMA scaffolds. Figure 5a presents the live/dead assay of cell-laden B-GelMA during a 2-week culture period. While cells readily integrate in the B-GelMA scaffolds through filling the interconnected microscale voids and adhere to the beads, permitting their spreading and proliferation in the complete course of culture (Figure 5b), the majority of encapsulated cells in the bulk GelMA do not survive the first day of culture (Figure 5c). Enhanced cell spreading on and among the beads in B-GelMA is presented in Figure 5d. The cell viability was quantified by normalizing the number of live cells with the total cell number, presented in Figure 5e. The B-GelMA scaffold affords ~ 100% cell viability; whereas, the cell viability on the bulk

GelMA ~ 0%. The metabolic activity of the cells, encapsulated in the scaffolds, measured using the PrestoBlue® assay (Figure 5f), demonstrate ~ 3.4, 8.5, 17.9, and 25.8 folds increase in days 3, 5, 7, and 14 post seeding, respectively, attesting to the enhanced proliferation.

Cell seeding from the scaffold surface inward was studied by placing a droplet of HUVECs (~5×10^4 cells) on the annealed/crosslinked scaffolds, presented schematically in Figure 6a. The droplet was allowed to be uptaken by the scaffold for ~ 5 min, followed by 3D confocal imaging. Figure 6b presents the 3D projection of B-GelMA and GelMA scaffolds from side and orthographic views. As can be seen in these images, immediate 3D cell seeding, i.e., penetration inside the B-GelMA takes place; whereas, the bulk GelMA scaffolds do not permit cell penetration. The fast penetration of cells inside the B-GelMA scaffolds may be a result of capillary forces among the beads, enhancing cell transportation via convection. Such enhanced delivery within a scaffold enabled by the interconnected microporosity may enable the rapid infiltration of cells inside B-GelMA, as universal scaffolds for advanced applications, such as time-sensitive cell culture (e.g., neonatal cardiomyocyte for cell therapy post myocardial infarction) and a broad range of co-culture systems, including the vascularization of bone and tumor models.

Conclusions

Regulating cellular behavior and function using chemical and biological cues of naturally-derived materials demands fine tuning of their mechanical and structural properties. Incorporating cells in chemically-modified bulk 3D hydrogel scaffolds permits improved cellcell and cell-matrix interactions in a microenvironment that mimics ECM. However, bulk hydrogels with high stiffness and small pore size are detrimental to cells, preventing inward oxygen and nutrient diffusion and cell-matrix migration, proliferation and integration. We have introduced a novel hydrogel platform based on annealing tens of micrometer-sized beads made up of a chemically-modified naturally-derived protein, GelMA, readily allowing for orthogonal physical and chemical dual crosslinking. Temperature-driven physical crosslinking of the beads enables the facile purification of gel building blocks without further chemical reaction, overcoming some of the challenges of newly-emerging beaded scaffolds, including oxygen-mediated impaired crosslinking. Beaded GelMA (B-GelMA) provides remarkable cell viability, adhesion, proliferation, and immediate 3D seeding, which would otherwise be impossible at a high concentration of bulk GelMA. This technology may be extended to other heat-responsive materials, setting the stage for transforming bulk to beaded scaffolds with independent control of microporosity from stiffness through a facile microfluidic strategy.

Acknowledgments

A. S. would like to acknowledge the financial support from the Canadian Institutes of Health Research (CIHR) through a postdoctoral fellowship. A. K. would like to acknowledge funding from the National Institutes of Health (HL137193, 5R01AR057837, 1R01EB021857). D. D. would like to acknowledge funding from the Presidential Early Career Award for Scientists and Engineers (N00014-16-1-2997).

References

[1]. Peppas NA, Hilt JZ, Khademhosseini A, Langer R, Hydrogels in biology and medicine: from molecular principles to bionanotechnology, Adv. Mater 18 (2006) 1345–1360.

[2]. Drury JL, Mooney DJ, Hydrogels for tissue engineering: scaffold design variables and applications, Biomaterials. 24 (2003) 4337–4351. [PubMed: 12922147]

[3]. Caló E, Khutoryanskiy VV, Biomedical applications of hydrogels: A review of patents and commercial products, Eur. Polym. J 65 (2015) 252–267.

[4]. Bouhadir KH, Lee KY, Alsberg E, Damm KL, Anderson KW, Mooney DJ, Degradation of partially oxidized alginate and its potential application for tissue engineering, Biotechnol. Prog. 17 (2001) 945–950. doi:10.1021/bp010070p. [PubMed: 11587588]

[5]. Hoffman AS, Hydrogels for biomedical applications, Adv. Drug Deliv. Rev 64 (2012) 18–23.

[6]. Leijten J, Seo J, Yue K, Trujillo-de Santiago G, Tamayol A, Ruiz-Esparza GU, Shin SR, Sharifi R, Noshadi I, Álvarez MM, Spatially and temporally controlled hydrogels for tissue engineering, Mater. Sci. Eng. R Reports 119 (2017) 1–35.

[7]. Yang J, Zhang YS, Yue K, Khademhosseini A, Cell-laden hydrogels for osteochondral and cartilage tissue engineering, Acta Biomater. 57 (2017) 1–25. [PubMed: 28088667]

[8]. Ahadian S, Khademhosseini A, Smart scaffolds in tissue regeneration, Regen. Biomater. 5 (2018) 125–128. [PubMed: 29977595]

[9]. Zhang YS, Khademhosseini A, Advances in engineering hydrogels, Science (80-.). 356 (2017) eaaf3627.

[10]. Ooi HW, Hafeez S, van Blitterswijk CA, Moroni L, Baker MB, Hydrogels that listen to cells: a review of cell-responsive strategies in biomaterial design for tissue regeneration, Mater. Horizons. 4 (2017) 1020–1040.

[11]. Brown TE, Anseth KS, Spatiotemporal hydrogel biomaterials for regenerative medicine, Chem. Soc. Rev 46 (2017) 6532–6552. [PubMed: 28820527]

[12]. Lu W, Le X, Zhang J, Huang Y, Chen T, Supramolecular shape memory hydrogels: a new bridge between stimuli-responsive polymers and supramolecular chemistry, Chem. Soc. Rev 46 (2017) 1284–1294. [PubMed: 28138679]

[13]. Tam RY, Smith LJ, Shoichet MS, Engineering cellular microenvironments with photo-and enzymatically responsive hydrogels: Toward biomimetic 3D cell culture models, Acc. Chem. Res 50 (2017) 703–713. [PubMed: 28345876]

[14]. Lu Y, Aimetti AA, Langer R, Gu Z, Bioresponsive materials, Nat. Rev. Mater 2 (2017) 16075.

[15]. Nakamura H, Lee AA, Afshar AS, Watanabe S, Rho E, Razavi S, Suarez A, Lin Y-C, Tanigawa M, Huang B, Intracellular production of hydrogels and synthetic RNA granules by multivalent molecular interactions, Nat. Mater 17 (2018) 79. [PubMed: 29115293]

[16]. Sun TL, Kurokawa T, Kuroda S, Bin Ihsan A, Akasaki T, Sato K, Haque MA, Nakajima T, Gong JP, Physical hydrogels composed of polyampholytes demonstrate high toughness and viscoelasticity, Nat. Mater 12 (2013) 932. [PubMed: 23892784]

[17]. Rosales AM, Anseth KS, The design of reversible hydrogels to capture extracellular matrix dynamics, Nat. Rev. Mater 1 (2016) 15012. [PubMed: 29214058]

[18]. Khademhosseini A, Langer R, Microengineered hydrogels for tissue engineering, Biomaterials. 28 (2007) 5087–5092. [PubMed: 17707502]

[19]. Chung BG, Lee K-H, Khademhosseini A, Lee S-H, Microfluidic fabrication of microengineered hydrogels and their application in tissue engineering, Lab Chip. 12 (2012) 45–59. [PubMed: 22105780]

[20]. Annabi N, Nichol JW, Zhong X, Ji C, Koshy S, Khademhosseini A, Dehghani F, Controlling the porosity and microarchitecture of hydrogels for tissue engineering, Tissue Eng. Part B Rev 16 (2010) 371–383. [PubMed: 20121414]

[21]. Nichol JW, Koshy ST, Bae H, Hwang CM, Yamanlar S, Khademhosseini A, Cell-laden microengineered gelatin methacrylate hydrogels, Biomaterials. 31 (2010) 5536–5544. [PubMed: 20417964]

[22]. Aubin H, Nichol JW, Hutson CB, Bae H, Sieminski AL, Cropek DM, Akhyari P, Khademhosseini A, Directed 3D cell alignment and elongation in microengineered hydrogels, Biomaterials. 31 (2010) 6941–6951. [PubMed: 20638973]

[23]. De Gennes P-G, Gennes P-G, Scaling concepts in polymer physics, Cornell university press, 1979.

[24]. Li W, Zhang L, Ge X, Xu B, Zhang W, Qu L, Choi C-H, Xu J, Zhang A, Lee H, Microfluidic fabrication of microparticles for biomedical applications, Chem. Soc. Rev 47(2018) 5646–5683. [PubMed: 29999050]

[25]. Griffin DR, Weaver WM, Scumpia PO, Di Carlo D, Segura T, Accelerated wound healing by injectable microporous gel scaffolds assembled from annealed building blocks, Nat. Mater 14 (2015) 737–744. doi:10.1038/nmat4294. [PubMed: 26030305]

[26]. Sideris E, Griffin DR, Ding Y, Li S, Weaver WM, Di Carlo D, Hsiai T, Segura T, Particle Hydrogels Based on Hyaluronic Acid Building Blocks, ACS Biomater. Sci. Eng 2 (2016) 2034–2041. doi:10.1021/acsbiomaterials.6b00444.

[27]. Mealy JE, Chung JJ, Jeong HH, Issadore D, Lee D, Atluri P, Burdick JA, Injectable Granular Hydrogels with Multifunctional Properties for Biomedical Applications, Adv. Mater 30 (2018) 1–7. doi:10.1002/adma.201705912.

[28]. Krutkramelis K, Xia B, Oakey J, Monodisperse polyethylene glycol diacrylate hydrogel microsphere formation by oxygen-controlled photopolymerization in a microfluidic device, Lab Chip. 16 (2016) 1457–1465. [PubMed: 26987384]

[29]. Hoque ME, Nuge T, Yeow TK, Nordin N, Prasad R, Gelatin based scaffolds for tissue engineering-a review, Polym. Res. J 9 (2015) 15.

[30]. Santoro M, Tatara AM, Mikos AG, Gelatin carriers for drug and cell delivery in tissue engineering, J. Control. Release. 190 (2014) 210–218. [PubMed: 24746627]

[31]. Rose JB, Pacelli S, El Haj AJ, Dua HS, Hopkinson A, White LJ, Rose FRAJ, Gelatin-based materials in ocular tissue engineering, Materials (Basel). 7 (2014) 3106–3135. [PubMed: 28788609]

[32]. Gnavi S, Di Blasio L, Tonda-Turo C, Mancardi A, Primo L, Ciardelli G, Gambarotta G, Geuna S, Perroteau I, Gelatin-based hydrogel for vascular endothelial growth factor release in peripheral nerve tissue engineering, J. Tissue Eng. Regen. Med 11 (2017) 459–470. [PubMed: 24945739]

[33]. Pina S, Oliveira JM, Reis RL, Natural-based nanocomposites for bone tissue engineering and regenerative medicine: A review, Adv. Mater 27 (2015) 1143–1169. [PubMed: 25580589]

[34]. Yue K, Santiago GT, Alvarez MM, Tamayol A, Annabi N, Khademhosseini A, Synthesis, properties, and biomedical applications of gelatin methacryloyl (GelMA) hydrogels, Biomaterials. 73 (2015) 254–271. doi:10.1016/j.biomaterials.2015.08.045. [PubMed: 26414409]

[35]. Yue K, Li X, Schrobback K, Sheikhi A, Annabi N, Leijten J, Zhang W, Zhang YS, Hutmacher DW, Klein TJ, Khademhosseini A, Structural analysis of photocrosslinkable methacryloyl-modified protein derivatives, Biomaterials. 139 (2017) 163–171. doi:10.1016/j.biomaterials.2017.04.050. [PubMed: 28618346]

[36]. Zhao X, Lang Q, Yildirimer L, Lin ZY, Cui W, Annabi N, Ng KW, Dokmeci MR, Ghaemmaghami AM, Khademhosseini A, Photocrosslinkable gelatin hydrogel for epidermal tissue engineering, Adv. Healthc. Mater 5 (2016) 108–118. [PubMed: 25880725]

[37]. Klotz BJ, Gawlitta D, Rosenberg AJWP, Malda J, Melchels FPW, Gelatin-methacryloyl hydrogels: towards biofabrication-based tissue repair, Trends Biotechnol. 34 (2016) 394–407. [PubMed: 26867787]

[38]. Sheikhi A, de Rutte J, Haghniaz R, Akouissi O, Sohrabi A, Di Carlo D, Khademhosseini A, Modular hydrogels from macromolecules with orthogonal thermo-chemical responsivity: Microfluidic fabrication and characterization, MethodsX. Submitted (2018).

[39]. Danks AE, Hall SR, Schnepp Z, The evolution of ‘sol-gel’chemistry as a technique for materials synthesis, Mater. Horizons. 3 (2016) 91–112.

[40]. Ninan G, Joseph J, Aliyamveettil ZA, A comparative study on the physical, chemical and functional properties of carp skin and mammalian gelatins, J. Food Sci. Technol 51 (2014)2085–2091. [PubMed: 25190867]

[41]. Chen Q-Z, Bismarck A, Hansen U, Junaid S, Tran MQ, Harding SE, Ali NN, Boccaccini AR, Characterisation of a soft elastomer poly(glycerol sebacate) designed to match the mechanical properties of myocardial tissue, Biomaterials. 29 (2008) 47–57. doi:10.1016/j.biomaterials.2007.09.010. [PubMed: 17915309]

[42]. Kaiser NJ, Coulombe KLK, Physiologically inspired cardiac scaffolds for tailored in vivo function and heart regeneration, Biomed. Mater 10 (2015) 34003.

[43]. Shaw JM, Hamad NM, Coleman TJ, Egger MJ, Hsu Y, Hitchcock R, Nygaard IE, Intra-abdominal pressures during activity in women using an intra-vaginal pressure transducer, J. Sports Sci 32 (2014) 1176–1185. [PubMed: 24575741]

[44]. Zuidema JM, Rivet CJ, Gilbert RJ, Morrison FA, A protocol for rheological characterization of hydrogels for tissue engineering strategies, J. Biomed. Mater. Res. Part B Appl. Biomater 102 (2014) 1063–1073. [PubMed: 24357498]

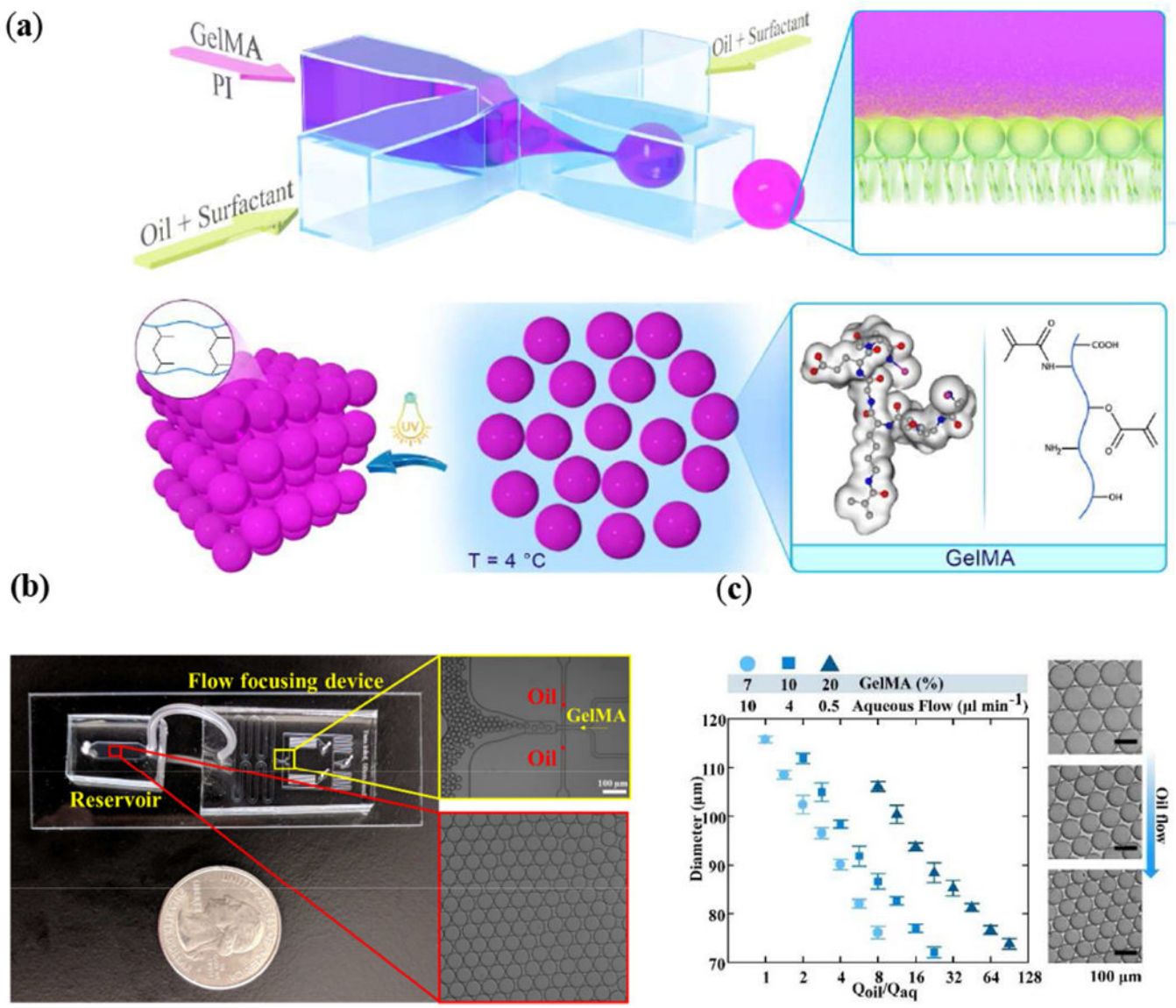

Figure 1. Microfluidic-assisted fabrication of beaded GelMA (B-GelMA).

(**a**) Schematic of surfactant-stabilized microbead production from a GelMA pre-polymer solution using a flow focusing microfluidic device, followed by purification in cold water (4 °C) to obtain stable physically-crosslinked GelMA microbeads. The microbeads may readily be crosslinked in the presence of photoinitiator to form an annealed microporous structure using UV light. Other viable crosslinking methods include visible light and redox pair-mediated fre-radical polymerization, commonly used to prepare bulk GelMA [37]. (**b**) Images of the flow focusing microfluidic device, comprising an inlet for the GelMA solution flow, pinching flow (oil/surfactant) inlets, and one outlet flow. The surfactant-stabilized beads were continuously monitored in an oil reservoir, followed by collecting them in a microcentrifuge tube and washing to remove the oil/surfactant. (**c**) GelMA bead size versus fluid (oil-to-water) flow ratio and GelMA concentration (7%, 10%, and 20 %w/v), showing

the versatility of the flow focusing technology in generating beads with sizes ~ 70-115 μm by altering the flow. The optical images show the beads made up of a 7% GelMA solution.

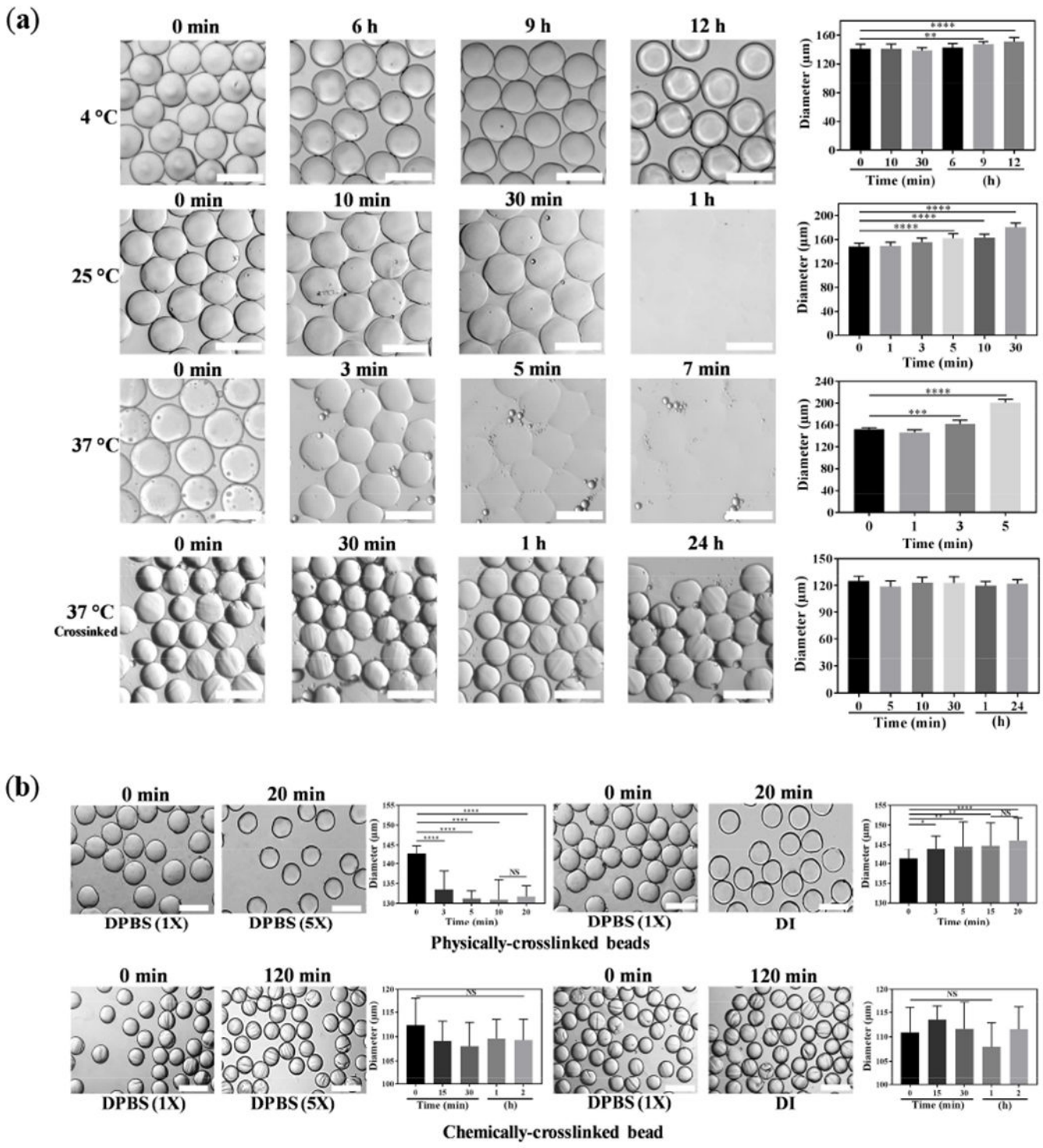

Figure 2. Stability and tailored swelling of GelMA beads.

(a) Stability of GelMA beads is investigated at varying temperatures over time. At 4 °C, GelMA is physically crosslinked, allowing for a long-term stability, which enables the facile processing of beads for a myriad of applications, such as crosslinking, annealing, and culturing cells. Increasing the temperature decreases the stability, resulting in the dissolution

of beads. Importantly, chemically-crosslinked beads withstand the physiological temperature for at least 24 h. (**b**) Tailored swelling and shrinking of GelMA beads are achieved through regulating the ionic strength gradient inside and outside the microbeads. When the physically-crosslinked beads containing 1× DPBS are placed in a 5× DPBS solution, they shrink, and when 1× DPBS-loaded beads are incubated in DI water, they swell (T = 4 °C). The chemically-crosslinked beads for 120 s do not undergo significant swelling and shrinking (T = 37 °C). The scale bars represent 200 μm.

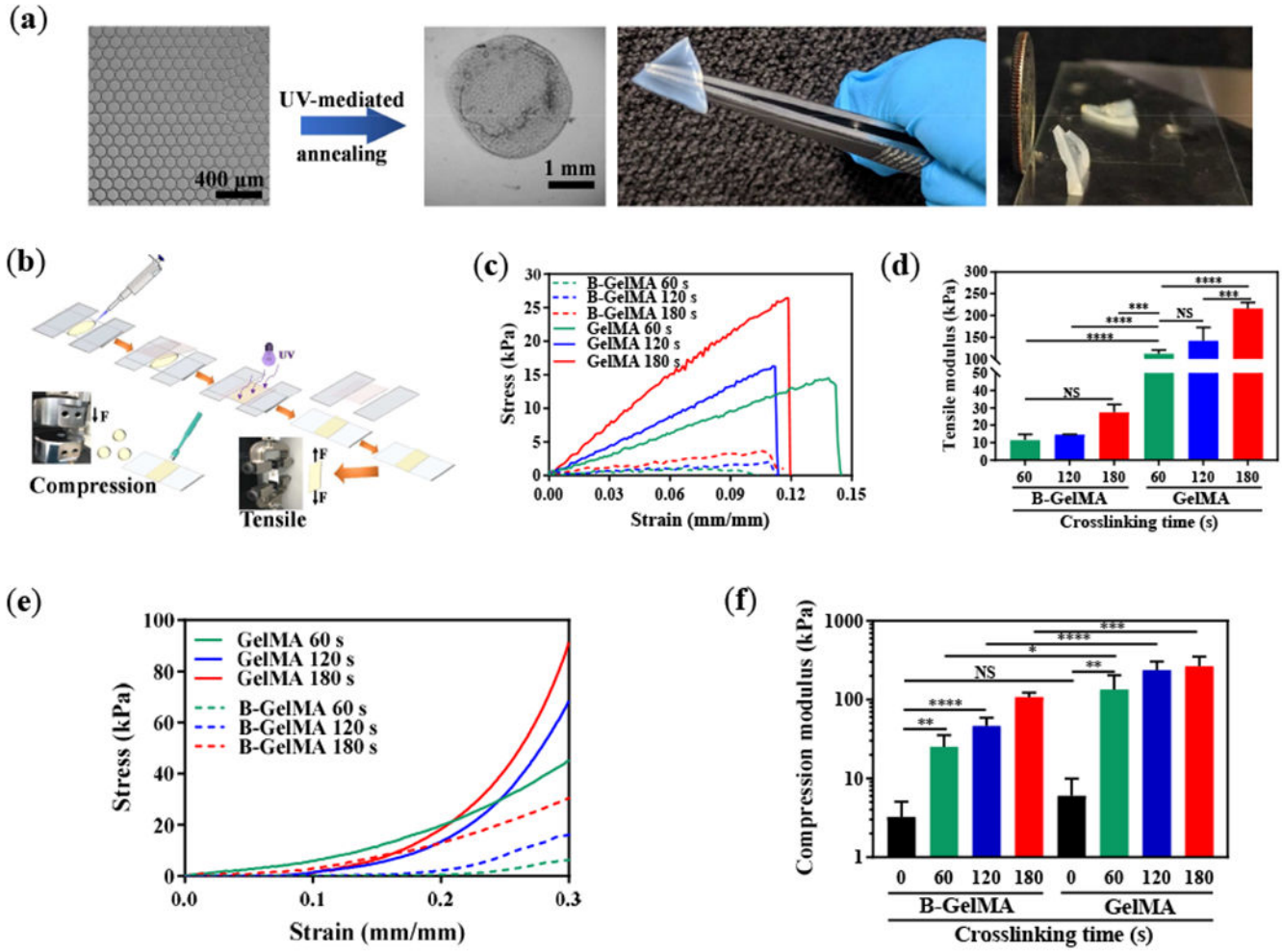

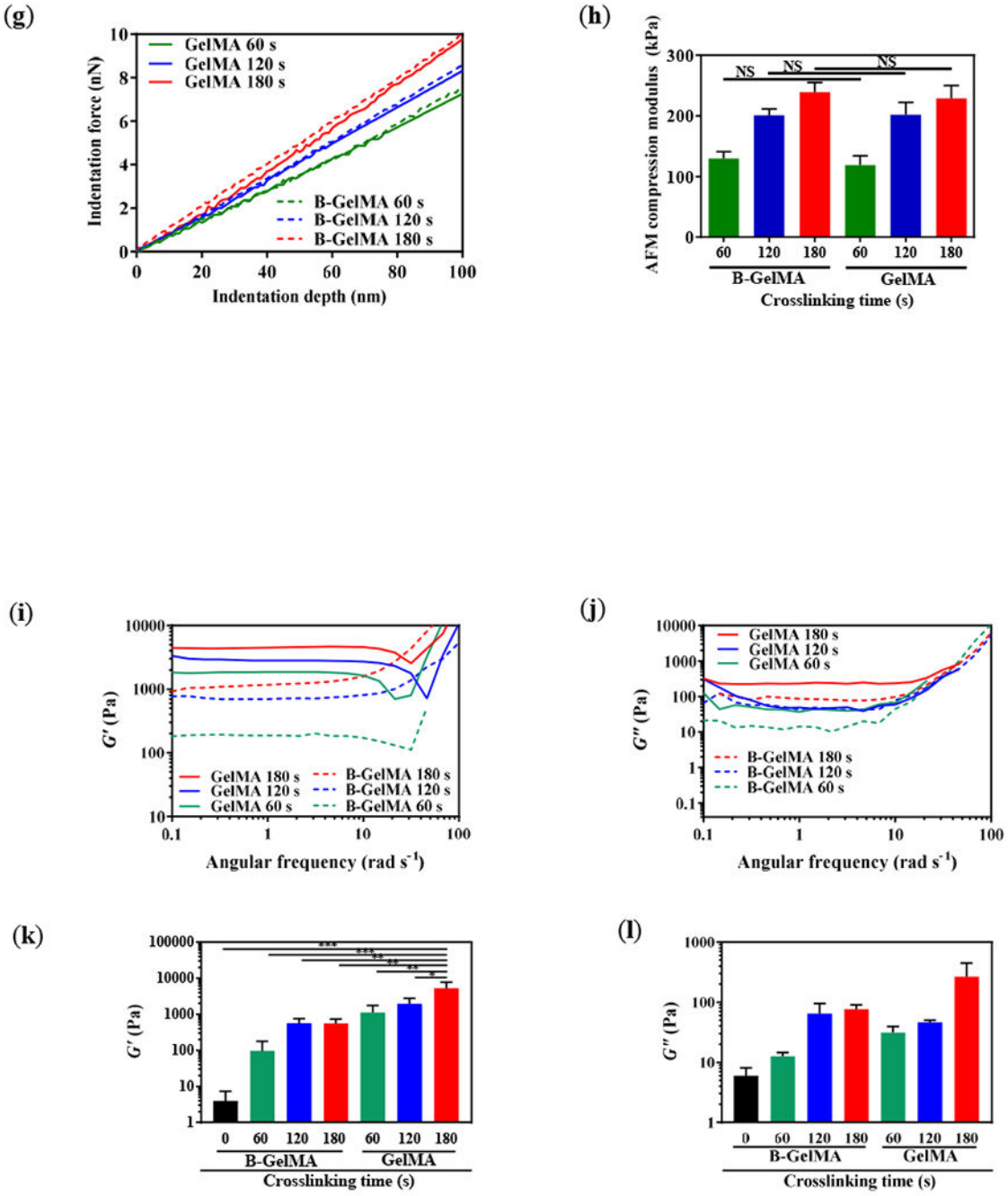

Figure 3. Annealing GelMA microbeads yields beaded GelMA (B-GelMA).

(**a**) UV light-mediated annealing of GelMA beads prepare from a 20% w/v GelMA solution in DPBS, resulting in intra- and inter-bead crosslinking, forming self-standing microporous B-GelMA scaffolds with a tailored number of packed bead layers. (**b**) Schematic of sample preparation for tensile and compression moduli characterization. (**c**) Tensile stress versus tensile strain, and (**d**) tensile moduli of B-GelMA and bulk GelMA, crosslinked using UV light (intensity ~ 10 mW cm^{-2} for 60 s, 120 s, and 180 s). Note that uncrosslinked beads were characterize as a control. (**e**) Compression stress versus compression strain, and (**f**)

compression moduli of B-GelMA and bulk GelMA, crosslinked as described in (**c**, **d**). (**g**) Atomic force microscopy (AFM) indentation force versus indentation depth for B-GelMA and GelMA. The small indentation depth (~ 100 nm) enables to probe the stiffness (compression moduli) (**h**) of individual beads as well as the bulk gel surface. Rheological properties of B-GelMA compared to the bulk GelMA in terms of storage (**i**) and loss (**j**) moduli versus angular frequency. A summary of storage and loss moduli at an angular frequency ~ 1 rad s^{-1} and strain ~ 0.1% is presented in (**k**) and (**l**), respectively.

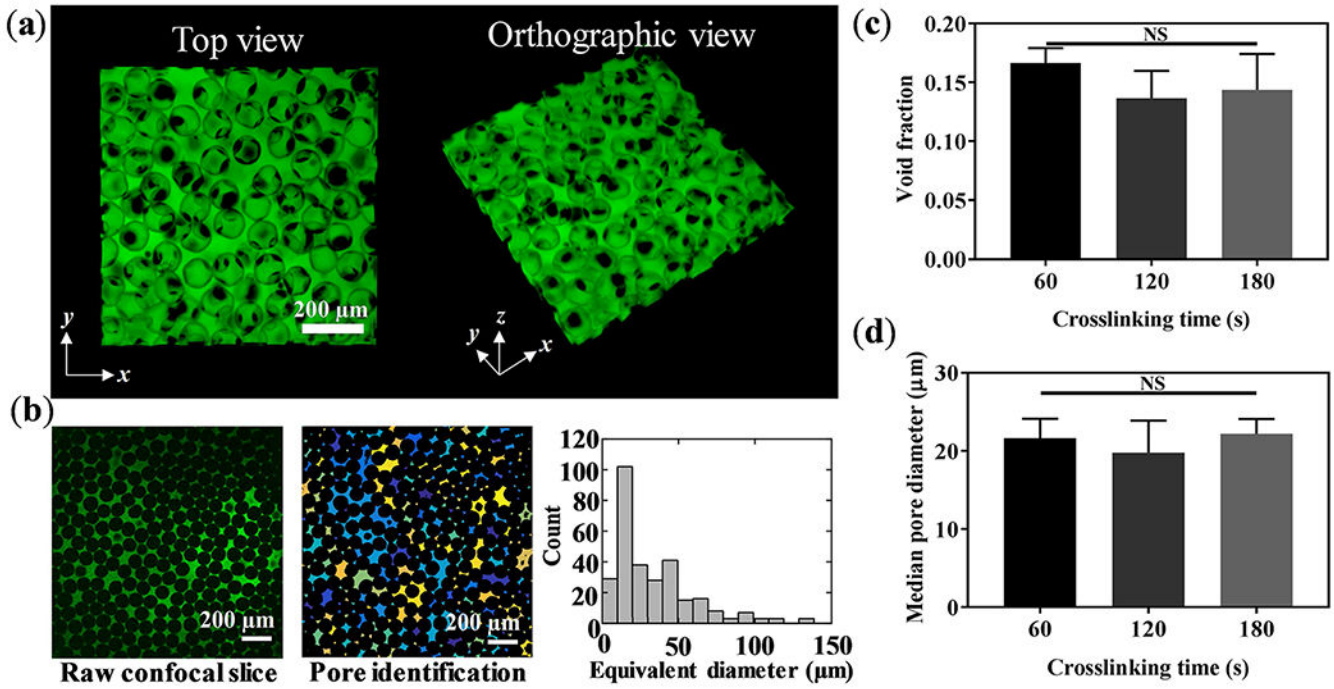

Figure 4. Pore characterization of B-GelMA.

(**a**) 3D confocal projection of B-GelMA scaffolds. Void space is imaged by incubating scaffolds in FITC-labeled dextran. (**b**) Process overview for pore size analysis. 2D slices were analyzed using a custom-built MATLAB algorithm to detect void spaces between the annealed beads. Void area was converted to circles of equal area to extrapolate equivalent diameter. (**c**) Void space fraction for B-GelMA scaffolds, prepared using varying crosslinking times, i.e., varying matrix stiffness. (**d**) Median pore diameter of B-GelMA scaffolds versus crosslinking time. The porosity and void fraction of B-GelMA scaffolds are independent of the matrix stiffness. Accordingly, B-GelMA generates a protein-based microporous scaffold with orthogonal porosity and stiffness.

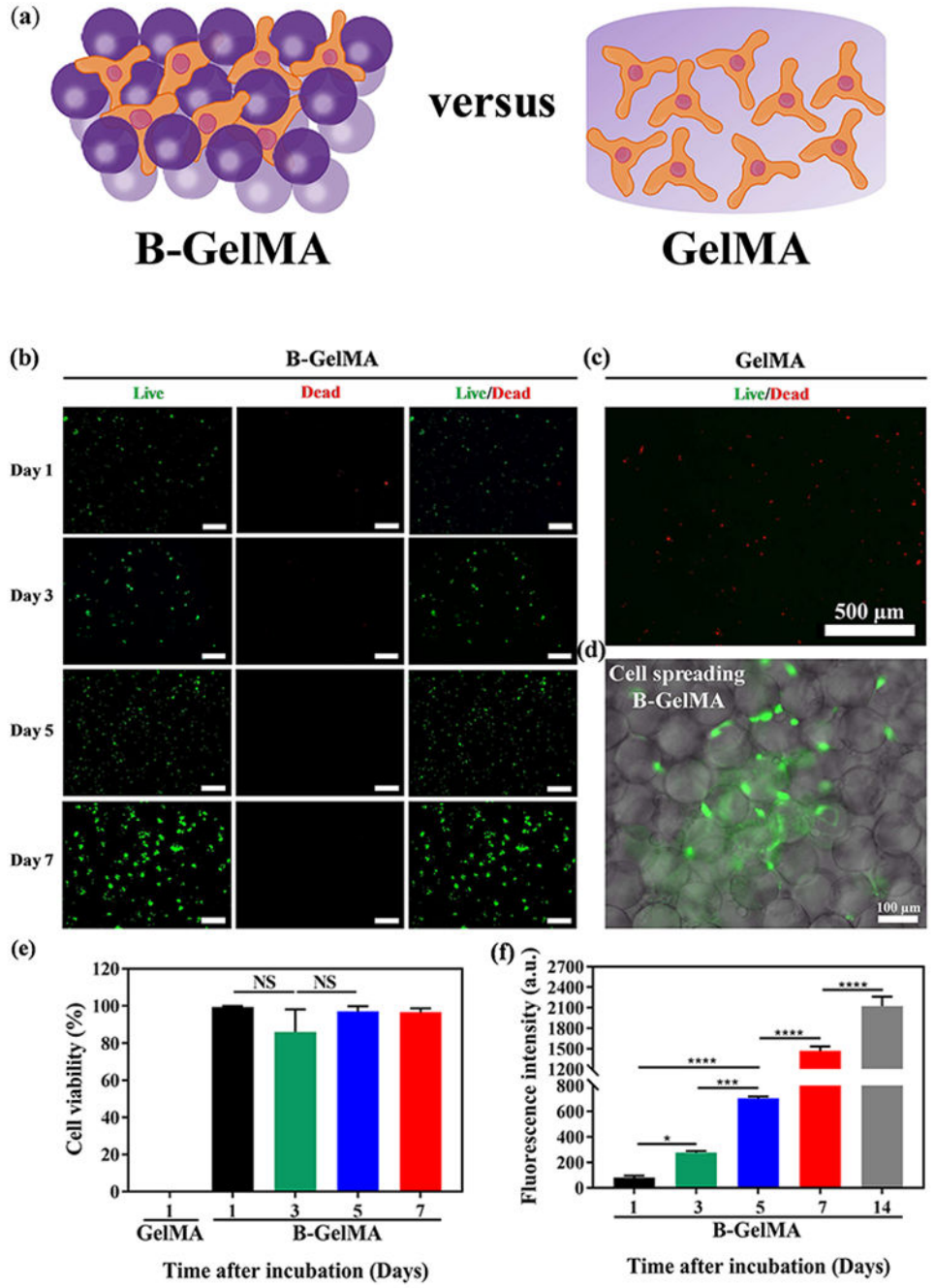

Figure 5. B-GelMA provides a microporous scaffold with independent stiffness and pore size for 3D cell culture.

(**a**) Schematic of 3D cell culture in B-GelMA versus bulk GelMA. (**b**) Assessment of live (green) and dead (red) cells, showing that the 3D encapsulation of NIH/3T3 fibroblasts in B-GelMA scaffolds with a high polymer concentration (20% w/v) results in high cell viability, excellent adhesion, and significant proliferation, compared to the bulk GelMA (**c**) in which cells do not survive the first day of culture. Scale bars are 500 μm. (**d**) Fluorescent microscopy image of cells adhering to the annealed GelMA beads and spreading among

them. (**e**) Cell viability, defined as the number of live cells divided by the total cell number for GelMA and B-GelMA, showing that while GelMA do not support cells, B-GelMA yields ~ 100% viability within an extended time. (**f**) Metabolic activity of the cells, measured using the PrestoBlue® assay, showing that B-GelMA affords an ~ 25-fold increase in the metabolic activity (proliferation) within 14 days. No metabolic activity was observed in the bulk GelMA.

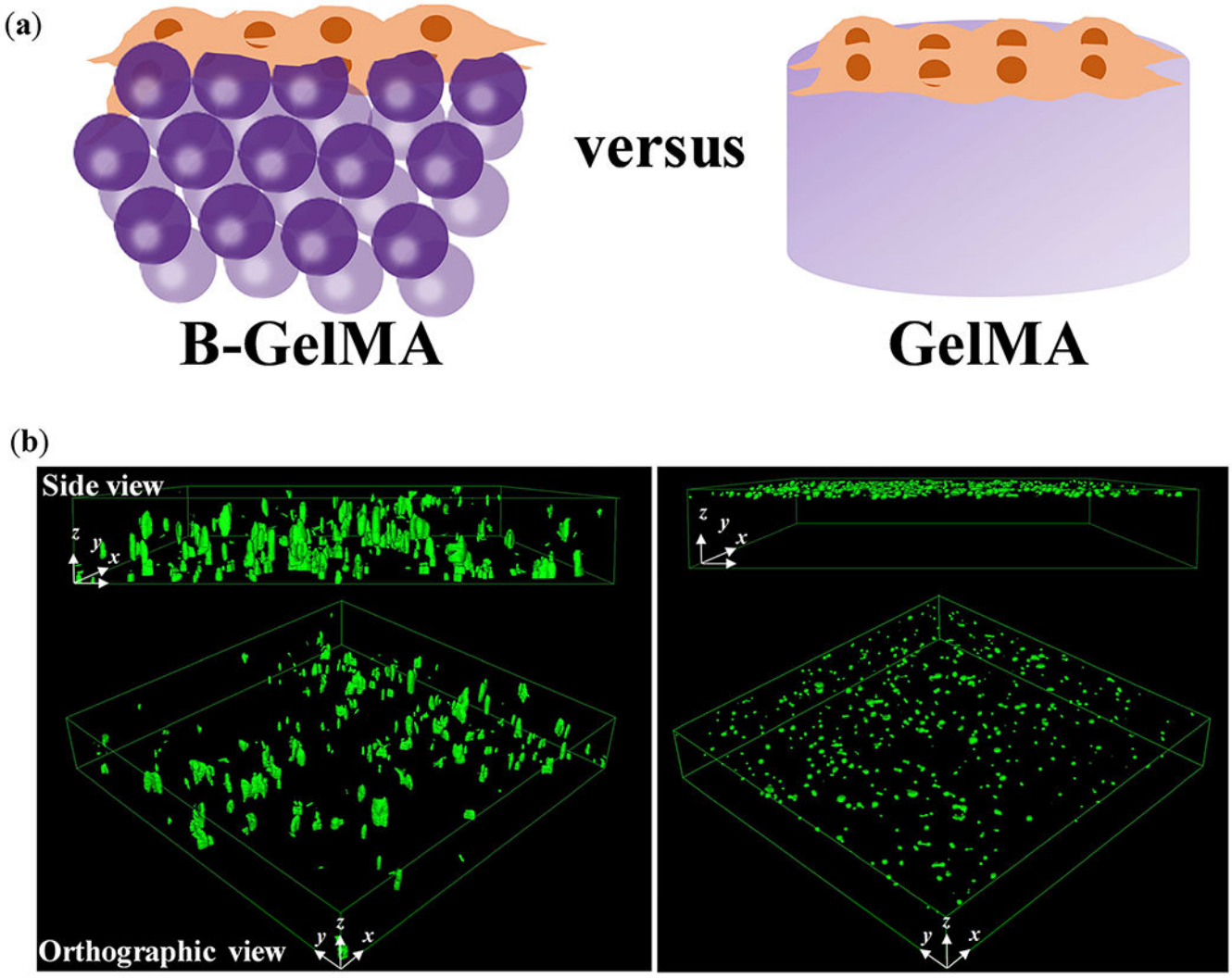

Figure 6. Three-dimensional cell seeding in B-GelMA versus bulk GelMA scaffolds.

(**a**) Schematic of cell seeding experiments wherein a concentrated HUVEC solution is placed on top of the pre-made scaffolds, followed by immediate confocal imaging. (**b**) HUVECs seeded on top of the B-GelMA readily transfer into the micropores of the scaffold in less than 5 min (left panel), shown in the confocal microscope images; whereas, the bulk GelMA (20% w/v) does not support immediate cell infiltration. B-GelMA scaffolds (thickness 0.5-1 mm) were seeded from the top and imaged from the bottom. Cells were able to penetrate all the way through the scaffold. The images only show a depth of field ~ 250 μm from the bottom. For the bulk gel, the scaffold thickness ~ 250 μm, and the image presents the whole 3D sample. Image dimensions ~ 1550 μm × 1550 μm × 254 μm.